Chalcogenide Letters Vol. 12, No. 6, June 2015, p. 313 - 323

STIMULATED LUMINESCENCE BEHAVIOR BY EMBEDDING ACTIVATED SILVER NANOPARTICLES IN TELLURITE GLASS

N.M.YUSOFF , M.R.SAHAR*
Advanced Optical Material Research Group, Department of Physics, Faculty of Science, Universiti Teknologi Malaysia, 81310 UTM Skudai, Johor, Malaysia.

A series of samarium doped magnesium tellurite glass embedded silver nanoparticles has successfully been prepared by melt quenching technique. The amorphous nature of the glass is determined by X-ray diffraction method while the existences of Ag NPs are confirmed using Transmission Electron Microscopy analysis. The optical measurements are performed by UV-Vis absorption and photoluminescence spectroscopy. It is found that the glass is amorphous in nature while the TEM image displays the randomly oriented spherical and non-spherical silver NPs with an average size of about 17 nm in diameter. From the UV-Vis absorption spectra, the surface plasmon resonance (SPR) peaks are detected at 550 and 578 nm while from the PL spectra, a single emission band for each composition which corresponds to $^4G_{5/2} \rightarrow {}^6H_{11/2}$ transition is observed under an excitation of 554 nm. The intensity of this transition enhances as the concentration of AgCl is increased up to 0.4 mol%. Meanwhile the Q-factor increases with the increasing of up to 0.4 mol% AgCl which indicates the phonon loss through the non-radiative emission is reduced. At this composition, the decay lifetime reduces which indicate that the energy transfer from Ag NPs to Sm^{3+} ions have effectively taken place, resulted in a small dissipation of energy. On the other hand, beyond 0.4 mol% AgCl, the Q-factor is decreased while the decay lifetime is increased.

(Received April 8, 2015; Accepted June 16, 2015)

Keywords: Glasses; X-ray diffraction; Electron microscopy; Optical properties; Luminescence

1. Introduction

Metallic nanoparticles (NPs) have different characteristics from those of bulk metals and therefore are under immense investigations [1-11]. In bulk metals the electrons are least confined due to the overlapping of conduction and valence band, therefore they have conducting behaviour. However as the separation between conduction and valence band is increased the electrons are more confined. In case of metallic NPs due to the confinement of electrons many novel and noticeable phenomena are likely to happen.

Surface plasmon resonance (SPR) is a collective oscillation of free conduction electron that occurs at the surface of metal-dielectric media with opposite signs of dielectric constants. The surface plasmon wave (SPW) refers to the charge density wave under resonance condition whereas the frequency of light photons matches the natural frequency of surface electrons the field vectors reach their maxima at the interface of both media [12-13]. The field of plasmonic is the novel growing branch of science in which the optical characteristics and potential applications of metallic NPs are understood [4-6].

Some of the rare earth (RE) doped glasses may exhibit some unwanted effects such as concentration quenching due to the energy-transfer to neighboring ions. So in order to enhance the luminescence efficiency and remove this drawback, several methods can be adopted. Quite

*Corresponding author: mrahim057@gmail.com

recently, the embedding of metallic NPs inside the glass host resulted in the changing of the environment felt by the RE ions [7-11]. Samarium is one of the important active ions in rare earth family which exhibits strong orange-red luminescence in the visible region. The influence of Sm^{3+} ions in luminescence properties either down or up conversion phenomena has widely been studied in various based glasses [14]. However, the effect of Sm^{3+} embedded Ag NPs on the optical properties is not fully understood.

Heavy metal oxide (HMO) glasses are studied mainly due to their low phonon energy for laser application. Some of the HMO glasses include tellurite, lead, bismuth and germinate [15-19] has been investigated. Recently the study on Er^{3+} doped silver NPs embedded in tellurite glasses [20-25] has been reported. However, only few reports are found in the literature in which the effect of embedding metallic NPs on the luminescence properties of Sm^{3+} ions in tellurite glass has been studied [26]. Thus, it is the aim of this work to report the effect of Sm^{3+} doped magnesium tellurite glass embedded with Ag NPs on the enhancement of visible region luminescence emission of the glass.

2. Experimental

15 grams batch of bulk glass based on the composition of (89-x)TeO_2-(10)MgO-(1)Sm_2O_3-(x)AgCl with $0 \leq x \leq 0.6$mol% are prepared by the conventional melt-quenching technique. The use of AgCl instead of $AgNO_3$ is preferable since the melting temperature of AgCl is much closer to the melts temperature. A proportional amount of TeO_2 (purity ≥ 99%), MgO (99.9%), Sm_2O_3 (99+%), and AgCl (99.999%) are mixed in a platinum crucible before being melted in an electric furnace at 900°C for about 1 hour. The melts is then quenched on a pre-heated brass plate at 300°C and subsequently annealed at this temperature for 3 hours before being allowed to slowly cool down to room temperature. A sample without Sm^{3+} ions with 1 mol% of AgCl was also prepared to observe the SPR bands. The glass is then polished and cut with a thickness of 2.5 mm for optical measurements. Table 1 shows the nominal composition of the prepared glasses. All samples are visually transparent to the visible light.

Table 1.The nominal composition (mol%) of TeO_2-MgO-Sm_2O_3-AgCl glass system.

Sample identity	Nominal composition (mol%)			
	TeO_2	MgO	Sm_2O_3	AgCl
TMS	89.0	10.0	1.0	0.0
TMSA0.2	88.8	10.0	1.0	0.2
TMSA0.4	88.6	10.0	1.0	0.4
TMSA0.6	88.4	10.0	1.0	0.6
TMA	89.0	10.0	0.0	1.0

The glasses amorphisms are confirmed through X-Ray diffraction method. A relatively fine powder of glasses are prepared and then put in a sample holder. A Siemens Diffractometer D5000 is used to scan the sample from an angle of 10^o-80^o working at 30 kV and current 20 mA. The samples in the form of fine powder are prepared for the TEM measurement. A Philips CM12 with Docu Version 3.2 is being utilized. To obtain the best quality of the micrograph, the back scattered detector is being used. The absorption spectra are obtained with Shimadzu UV-3101PC UV-VIS-NIR scanning spectrophotometer in the range of 200-2000 nm. Meanwhile, the photoluminescence spectra are recorded upon excitation with a xenon flash lamp as the excitation source. The luminescence signal is analysed using a Monk-Gillieson type monochromator in combination with the photodiode detector at excitation wavelength of 554 nm. The system is operated at 1 nm resolution. The lifetime measurement is calculated from the obtained emission peak using second order experimental decay curve. All the errors are due to the experimental and instrumental which has been estimate to be around ± 5%.

3. Results and discussion

3.1 X-ray diffraction

Fig. 1 shows a typical powder X-Ray diffraction pattern for TMS and TMSA0.2 glass sample. From that figure, the appearance of a broad hump is observed, which confirms that the glass is amorphous in nature. The broad hump of TMSA0.2 is slightly narrower than TMS due to the embedment of nanoparticles in the glass matrix.

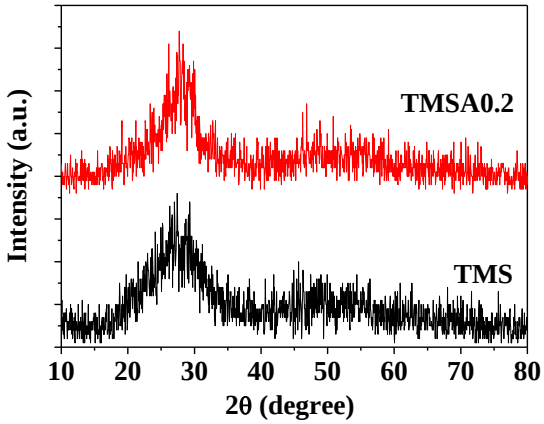

Fig.1. A typical X-Ray diffraction pattern for TMS and TMSA0.2 glass.

3.2 Formation of Ag NPs in glass matrix

The introduction of Ag NPs into the glass is reported to influence some of their optical and structural properties. Ag NPs are formed by the reduction of Ag ions (Ag^{+}) to the neutral state (Ag species) as ($Ag^{+}+1e^{-}\rightarrow Ag^{0}$) during the melting process then were freezed in the glass matrix during the cooling process [27] as in the case of $AgNO_3$ NPs reported by Malta et al. [28]. Figure 2 shows a TEM image for the glass containing Ag NPs. From Fig. 2, it can be seen that spherical and non-spherical particles of Ag NPs are dispersed homogeneously in the glass matrix with an average diameter size of about 17 nm. Since two shapes of Ag NPs are observed, this indicates that there are two type of polarisation which are transverse and longitudinal [29-32].

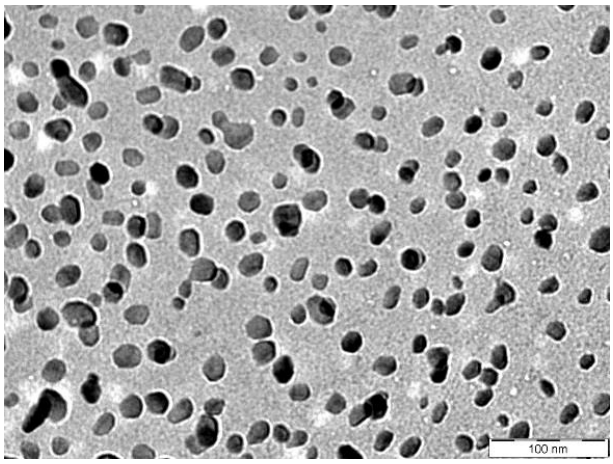

Fig.2. A TEM image for the glass containing 0.4 mol% Ag NPs. The average diameter is around 17 nm.

3.3 Optical absorption

The absorption analysis in the UV-Vis spectrum is the most reliable tool to study the function of metallic nanoparticles in the glass and to observe the existence of surface plasmon resonance (SPR) band [20]. Figure 3 shows the absorption spectrum of glass without Sm^{3+}. Two SPR bands centred at 550 nm and 578 nm are observed corresponding to the transverse and the longitudinal SPR oscillations of the Ag NPs respectively. The SPR peaks are also been found to be significantly red shifted as compared to the classic one which is in the range of 410-420 nm [33]. This might be due to the higher refractive index of the most tellurite glasses which normally lie approximately in the range of (2.0±0.1 to 2.5±0.1) [34-37]. It is known that the position of SPR is depending on refractive index. The higher the refractive index, the longer the SPR wavelength is [38-39]. It should however be noted that the intensities of both SPR peaks are not so immense. This is perhaps due to the existence of spherical and non-spherical types of Ag NPs in the glass matrix as appears in Fig. 2. Furthermore, the absorption coefficient of the samples is very much higher than those in the form of thin film as suggested by El-Hagary et al. [40].

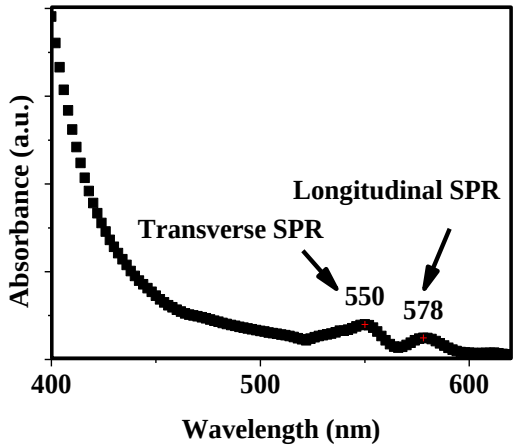

Fig.3. The absorption spectrum of glass without Sm^{3+} ion for TMA. There are two SPR bands, a transverse SPR located at 550 nm, and a longitudinal SPR located at 578 nm.

Figure 4 shows the absorption spectra of the Sm^{3+} doped glass at higher energy region. As can be seen, there are three absorption bands from UV-Vis region which correspond to the transition of $^6H_{5/2}$ to $^6P_{3/2}$ (400 nm), $^4I_{11/2}$ (470 nm), and $^4G_{5/2}$ (554 nm).The intensities of the peaks are low and such that the normalize intensity has been manipulated and inserted in that figure. From Figure 4, it can also be seen that only part of the predominantly transverse SPR appears in the UV-Vis absorption band at 550 nm. However, if a careful extrapolation is being made to this peak, it can clearly be seen that there is another SPR peak at 554 nm. Meanwhile, the absorption bands of the Ag NPs due to the longitudinal SPR (at 578 nm) do not appear in the glass containing Sm^{3+} ion. This is due to the low concentration of Ag NPs and an overlapping of longitudinal SPR band with the Sm^{3+} ion absorption band as reported by other workers [41]. Figure 5 shows the absorption spectra of the glass at lower energy region. As can be seen, seven absorption bands in NIR region can clearly be observed which are due to the transition from $^6H_{5/2}$ to $^6F_{11/2}$ (946 nm), $^6F_{9/2}$ (1084 nm), $^6F_{7/2}$ (1238 nm), $^6F_{5/2}$ (1384 nm), $^6F_{3/2}$(1490 nm), $^6H_{15/2}$(1550 nm) and $^6F_{1/2}$ (1592 nm). It is also observed that at this region the absorption intensity is slightly higher than that at the UV-Vis energy region. The reason for this is due to the transition from the ground state of $^6H_{5/2}$ to 6H and 6F are spin allowed (the total quantum number of spin, $\Delta S=0$) as has been reported by Ravi et al. [42]. In addition, it is interesting to note that the absorption intensity at lower energy is also slightly enhanced due to the insertion of Ag NPs. From Figure 5, it can be seen that only slightly peaks shift are observed which indicate the stability of glass network is almost maintained.

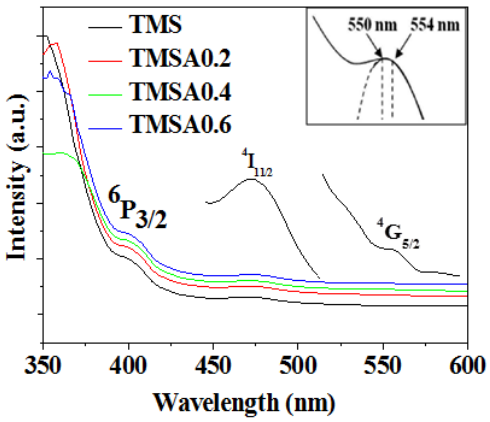

Fig.4. The absorption spectra of the glass at higher energy region. The inset shows the extrapolation of 550 nm SPR peak to the 554 nm absorption peak.

3.4 Photoluminescence properties

Fig. 6 shows the luminescence emission spectra of Sm^{3+} ions after taking the ackground reading into consideration on excitation with 554 nm radiations of a xenon flash lamp. From Figure 6, a single emission band for each composition is observed which is assigned to $^4G_{5/2} \rightarrow {}^6H_{11/2}$ transition and is located at higher wavelength compare to that of excitation wavelength. The intensity of this peak is rather weak due to the existence of two types of Ag NPs as has been discussed earlier. A re-plot of Figure 6 at a larger scale is shown in Figure 7. From Figure 7, it can be seen that the emission wavelength shifted from 724-722 as the AgCl is beyond 0.4 mol%. This is due to the contribution of energy transfer from Ag^0 to Sm^{3+} as well as the local field effect as will be described in the later section. If a plot of emission wavelength against the AgCl concentration is being made, a result as shown in Figure 8 can be obtained. From Figure 8 it can be seen that the emission energy is generally increased and reaches maximum at 0.4mol% of AgCl. The increase in emission energy shows that the energy loss due to the phonon vibration at this composition is at a minimum.

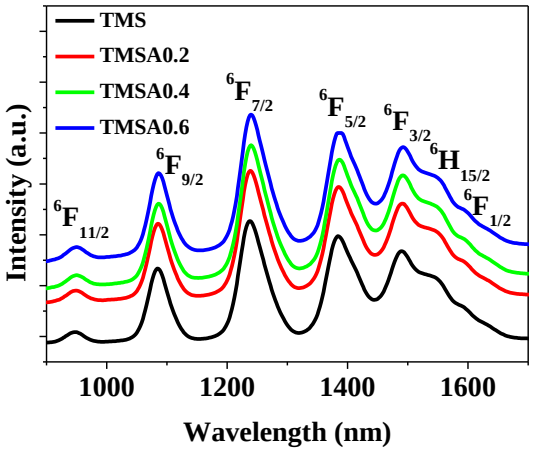

Fig.5. The absorption spectra of the glass at lower energy region.

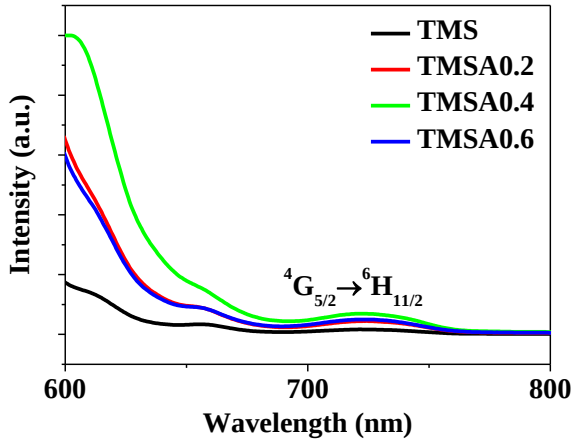

Fig.6. The down conversion emission spectra of Sm^{3+} ions on excitation with 554 nm radiations (after taking the background reading into consideration).

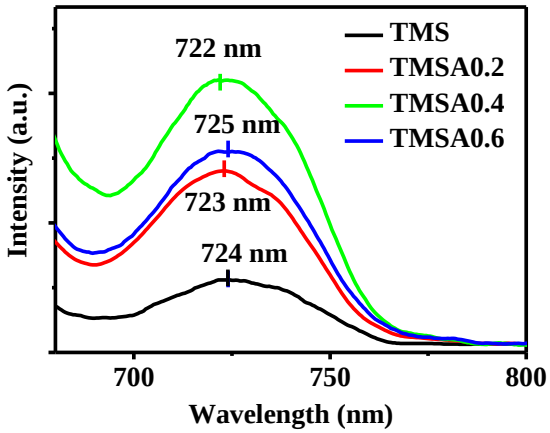

Fig.7. The emission band of $^4G_{5/2}\rightarrow{}^6H_{11/2}$ transition in a larger scale

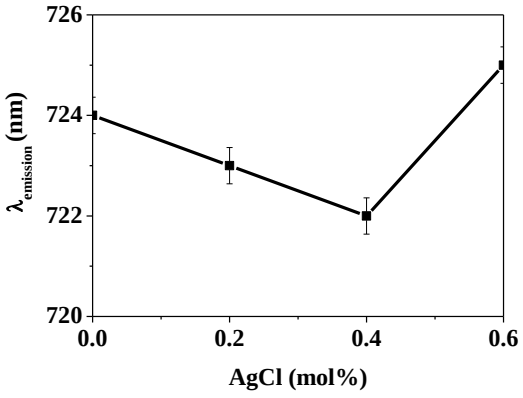

Fig.8. The emission wavelength against the AgCl concentration for $^4G_{5/2}\rightarrow{}^6H_{11/2}$ transition. The line is drawn as a guide for the eye.

Meanwhile Fig. 9 shows the variation of emission peak intensity for $^4G_{5/2}\rightarrow{}^6H_{11/2}$ transition as a function of AgCl concentration. From Figure 9, it is observed that the intensity increases as the AgCl concentration is increased with the highest number of photon emission occurs in TMSA0.4. It can also clearly be seen that the intensity is enhanced at least 3 times to the one without Ag NPs. This enhancement is attributed by two possible reasons: firstly is due to the local

field effect of Ag NPs in the vicinity of Sm^{3+} ions and secondly is due to an energy transfer (ET) between the Ag NPs and Sm^{3+} ions ($Ag^0 \rightarrow Sm^{3+}$) [43-44]. A similar enhancement has also been observed in the glass containing Eu^{3+} by Malta et al. [45-46] and Hayakawa et al. [46], thus supported the above argument.

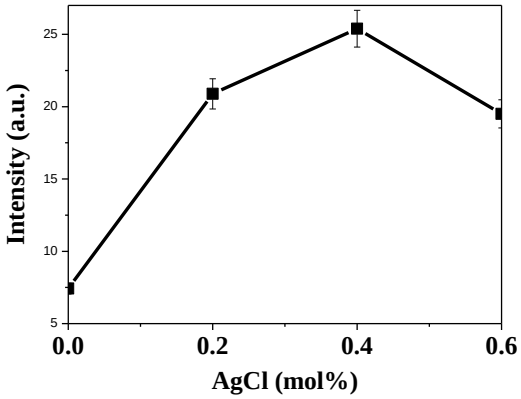

Fig.9. The emission intensity against the AgCl concentration for the $^4G_{5/2} \rightarrow {}^6H_{11/2}$ transition. The line is drawn as a guide for the eye.

It should be noted out that the energy transfer between Ag^0 (Ag species) and Sm^{3+} ion are two folds ie: the enhancement effect and the quenching effect [44, 47-50]. The quenching effect of luminescence occurs when energy is transferred from Sm^{3+} to Ag species, while for the enhancement effect, the energy is transferred from Ag^0 to Sm^{3+} [51]. The quenching effect can be observed in sample with more than 0.4 mol% Ag NPs where the emission intensity is decreased.

Thus, the possible mechanism for Sm^{3+} emission can be explained through the partial energy diagram as shown in Figure 10. The process starts when the electron is excited from $^6H_{5/2}$ to higher excited state $^6P_{3/2}$. Plasmon energy of Ag NPs is transferred to the exited electron at $^6P_{3/2}$ state of Sm^{3+}. Since the $^6P_{3/2}$ level has comparatively a shorter lifetime, the electron decay non-radiatively (NR) to relaxation level $^4G_{5/2}$. The emission lines for all composition are very close (see Fig. 6) then for simplicity, it can be assumed that Sm^{3+} ion decay radiatively (R) from $^4G_{5/2}$ to $^6H_{11/2}$at 723 nm, which is the average of the wavelength. Meanwhile, in the intermediate energy level, there is an energy transfer between Sm^{3+} ions called co-operative energy transfer (CET) between $^4G_{5/2}$ and $^6P_{3/2}$.

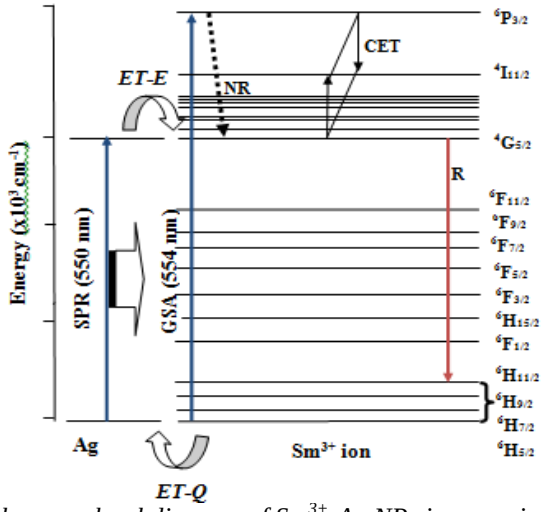

Fig.10.The partial energy level diagram of Sm^{3+}:Ag NPs in samarium doped magnesium tellurite glass embedded Ag NPs.

Furthermore, due to the difference between the relative permittivity of the metal and the surrounding glass matrix, this would allow the SPR to produce surface waves that move along the metal-dielectric interface. As a result, the electromagnetic energy will be concentrated more tightly, thus produce the giant electric field [7, 10] around the particle especially at a sharp metallic tip [51, 52]. Hence with respect to the incident field, a large local electric field is induced in the vicinity of lanthanide ions [10, 52].

The quality factor, Q which indicates the energy loss during the non-radiative transition can be calculated using equation [53],

$$Q = \frac{\lambda_{peak}}{FWHM} \tag{1}$$

where λ_{peak} is the wavelength at their respective bandwidth and FWHM (full width at half maxima) can be obtained from Figure 8.A plot of Q-factor as a function of Ag concentration can be made and the result is shown in Figure 11. From Figure 11, it can be seen that the Q-factor is generally increased as the AgCl concentration is increased. The result indicates that small energy has been dissipated to the surrounding during the transition which understandably is due to the phonon loss during the non-radiative emission. The reduction in energy lost resulted in the enhancement of luminescence of the glass. The decreasing in Q-factor beyond 0.4 mol% AgCl is due to the relatively higher amount of energy lost to the surrounding.

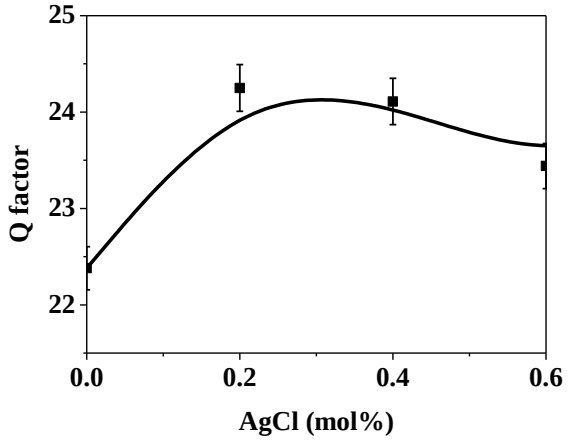

Fig.11. The plot of Q factor as a function of AgCl concentration for $^4G_{5/2} \rightarrow {}^6H_{11/2}$ *transition.The line is drawn as a guide for the eye.*

Fig. 12 shows the PL decay curve of S1 derived from single exponential rule monitored at emission wavelength 724 nm. All decay curve are well fitted by a second-order exponential equation [54-55],

$$I(t) = I_0 + A_1 \exp\left(\frac{-t}{\tau_1}\right) + A_2 \exp\left(\frac{-t}{\tau_2}\right) \tag{2}$$

where$I$ is PL intensity, $A_1$and $A_1$are constants, $t$is time,τ_1 and τ_2 are the rapid and slow lifetime for exponential components respectively and t is time. The decay time, τ is calculated using the relation [54-55],

$$\tau = \frac{A_1\tau_1^2 + A_2\tau_2^2}{A_1\tau_1 + A_2\tau_2} \tag{3}$$

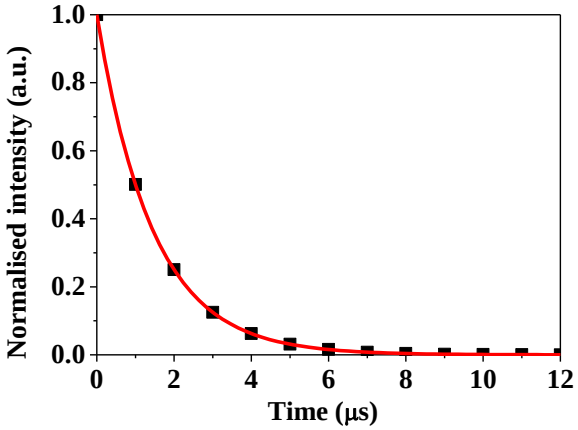

Fig.12. PL decay curve of (a) TMS at 724 nm

If a plot of decay time against the AgCl is made, the result as shown in Figure 13 can be obtained. It can be seen that, the decay lifetime decreases as AgCl is increased. However, beyond 0.4 mol% AgCl, the decay lifetime increases. This reduction indicates that the energy transfer from Ag^0 to Sm^{3+} ions has effectively taken place which resulted in the small dissipation of energy to surrounding. On the other hand, beyond 0.4 mol% AgCl, the decay lifetime is increased while the Q-factor is decreased.

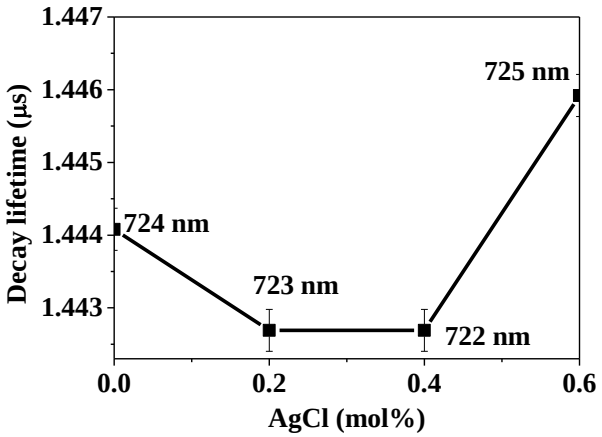

Fig.13. Decay lifetime as a function of AgCl concentration.
The line is drawn as a guide for the eye.

4. Conclusion

The samarium doped magnesium tellurite glass embedded with Ag NPs has successfully been prepared by conventional melt quenching technique. The XRD result shows that the glass is amorphous in nature. The formation of spherical and non-spherical shape of Ag NPs in the glass matrix with an average diameter around 17 nm is evidenced by the TEM image. The UV-Vis absorption spectra show that the SPR bands of the Ag NPs are located at 550 nm and 578 nm. The photoluminescence down conversion of the glass excited at 554 nm radiation shows the enhancement of emission in the red region. Such enhancement is attributed to the local field effect and energy transfer from Ag^0 to Sm^{3+}. It is also observed that the highest Q-factor occurs at 0.4 mol% AgCl which is attributed to the largest luminescent enhancement and the smallest decay lifetime.

Acknowledgements

The authors wish to acknowledge the financial support from Ministry of Higher Education through research grant of ERGS Vot4L032 and Universiti Teknologi Malaysia. The authors would also like to thanks Dr. R. J. Amjad for his assistances.

References

[1] A. M. Schwartzberg and J. Z. Zhang, J. Phys. Chem. C **112**, 10323 (2008).
[2] X. Lu, M. Rycenga, S. E. Skrabalak, B. Wiley, Y. Xia, Ann. Rev. Phys. Chem. **60,** 167 (2009).
[3] M. Bäumer, H.–J. Freund, Prog. Surf. Sci. **61**, 127 (1999).
[4] E. Ozbay, Science, **311**, 189 (2006).
[5] P. N. Prasad, Nanophotonics, Wiley, New Jersey (2004) p. 129.
[6] W. A. Murray, W. L. Barnes, Adv Mater. **19**, 3771 (2007).
[7] S. A. Maier, H. A. Atwater, J. Appl. Phys. **98**, 011101 (2005).
[8] W. L. Barnes, A. Dereux and T. W. Ebbesen, Nature **424**, 824 (2003).
[9] F. Le, D. W. Brandl, Y. A. Urzhumov, H. Wang, J. Kundu, N. J. Halas, J. Aizpurua, P.Nordlander, ACS Nano **2**, 707 (2008).
[10] S. Lal, S. Link, N. J. Halas, Nat. Photonics **1**, 641 (2007).
[11] C. D. Geddes, J. R. Lakowicz, J. Fluoresc. **12**, 121 (2002) .
[12] H. Yuan, Z. Xiaosong, L.Bo, L.Mengzhen, S.Qingliang, W.Youwei and L.Lan, J. Rare Earth **32**, 1096 (2013).
[13] J. Homola, S. S. Yee and G. Gauglitz, Sensor Actuator B **54**, 3 (1999).
[14] S. Shanmugasundari, K. Marimuthu, M. Sivaraman, S. SurendraBabu, J. Lumin. **130,** 1313 (2010).
[15] G. Lakshminarayana, J. Qiu, M.G. Brik, I. V. Kityk, J. Phys. Condens. Matter **20,** 335106 (2008)
[16] P. Nachimuthu, R. Jagannathan, J Am. Ceram. Soc. **82**, 387 (1999).
[17] B. Klimesz, G. Dominiak-Dzik, P. Solarz, M. Z˙ el echower, W. Ryba-Romanowski, J. Alloys. Compd. **403**, 76 (2005).
[18] V. V. R. K. Kumar, A. K. Bhatnagar, R. Jagannathan, J. Phys. D.: Appl. Phys. **34,** 1563 (2001).
[19] M. R. Sahar, A. K. Jehbu, M. M. Karim, J. Non- Cryst. Solids **213 & 214,** 164 (1997).
[20] R. J. Amjad, M. R. Sahar, S. K. Ghoshal, M. R. Dousti, S. Riaz, B. A. Tahir, J. Lumin. **132**, 2714 (2012).
[21] M.R. Dousti, M. R. Sahar, R. J. Amjad, S.K. Ghoshal, A. Khorramnazari A. Dordizadeh Basirabad, A. Samavati Eur. Phys. J. D **66**, 237 (2012).
[22] M. R. Dousti, M. R. Sahar, S. K. Ghoshal, R. J. Amjad, R. Arifin, J. Non-Crys. Solids **358**, 2939 (2012).
[23] R. J. Amjad, M.R. Sahar, S.K. Ghoshal, M.R. Dousti, S. Riaz, A.R. Samavati, R. Arifin, S. Naseem, J. Lumin. **136**, 145 (2013).
[24] V. A. G. Rivera, Y. Ledemi, M. El-Amraoui, Y. Messaddeq, and E. Marega Jr., Optics Express **22**(17), 21122 (2014) -21136.
[25] V. A. G. Rivera, S. P. A. Osorio, Y. Ledemi, D. Manzani, Y. Messaddeq, L. A. O. Nunes, E. Marega Jr., Optics Express **18**(24), 25321 (2010).
[26] T. Som and B. Karmakar, Spectrochim. Acta A **75**, 640 (2010).
[27] M. R. Dousti, M. R. Sahar, R. J. Amjad, S. K. Goshal, A. Awang, J. Lumin. **143,** 368 (2013)
[28] O. L. Malta, R. A. Santa-Cruz, G. F. De Sa, F. Auzel, J. Lumin. **33**, 261 (1985).
[29] S. Link and M. A. El-Sayed, J. Phys. Chem. B **103**(40), 8410 (1999).
[30] P. K. Jain, S. Eustis, and M. A. El-Sayed, J. Phys. Chem. B **110** (37), 18243 (2006).
[31] A. Abbas, L. Tian, J. J. Morrissey, E. D. Kharasch, and S. Singamaneni, Adv. Funct. Mater. **23,** 1789 (2013).
[32] V. A. G. Rivera, Y. Ledemi, S. P. A. Osorio, D. Manzani, F. A. Ferri, J. L. Ribeiro Sidney,

L. A. O. Nunes, E. Marega Jr, J. Non-Crys. Solids **378**, 126 (2013).
[33] U. Kreibig, M. Vollmer, Optical Properties of Metal Clusters, Springer Verlag, NY, 1995.
[34] P. G. Pavani, S. Suresh, V. C. Mouli, Opt. Mater. **34**, 215 (2011).
[35] S. Sakida, T. Nanba, Y. Miura, Mater. Lett. **60**, 3413 (2006).
[36] P.G.Pavani, K.Sadhana, and V.C.Mouli, Physica B **406**, 1242 (2011).
[37] E.Yousef, M.Hotzel and C.Russel, J. Non-Cryst. Solids **342**, 82 (2004).
[38] T. Som and B. Karmakar, Nano Res. **2**, 607 (2009).
[39] P. Mulvaney, Langmuir **12**, 788 (1996).
[40] M. El-Hagary, M. Emam-Ismail, E. R. Shaaban, I. Shaltout, J. Alloys. Compd. **485,** 519 (2009).
[41] V. A. G. Rivera, Y. Ledemi, M. El-Amraoui, Y. Messaddeq and E. Marega Jr., Optic Express **22** (17), 021122 (2014).
[42] O. Ravi, C. Madhukar Reddy, L. Manoj, B. Deva Prasad Raju, J. Mol. Struc. **1029,** 53 (2012).
[43] M. V. Roldan, A. Frattini, O.de Sanctis, H. Troiani, N.Pellegri, Appl. Surf. Sci. **254,** 281 (2007).
[44] Z.Pan, A.Crosby, O.Obadina, A.Ueda, R.Aga, R.Mu, S.H.Morgan, MRS Sym.Proc. **1028**, 1208-O09-16 (2010).
[45] O. L. Malta and M. A. C. dos Santos, Chem. Phys. Lett. **174**, 13 (1990) -18.
[46] T. Hayakawa, S. T. Selvan, and M. Nogami, Appl. Phys. Lett. **74**, 1513 (1999).
[47] T.Som, B.Karmakar, J.Appl.Phys. **105**, 013102 (2009).
[48] C.B.de Araujo, L.R.P.Kassab, R.A.Kobayashi, L.P.Naranjo, and P.A.Santa Cruz, J.Appl.Phys.**99**, 123522 (2006).
[49] S.DeMarchi, G.Mattei, P.Mazzoldi, C.Sada, and A.Miotello, J.App.Phys. **92,** 4249 (2002).
[50] J.A.Jimenez, S.Lysenko, and H.Liu, J.Lumin.**128**, 831 (2007).
[51] V.A.G.Rivera, Y.Ledemi, S.P.A. Osorio, D.Manzani, Y.Messaddeq, L.A.O. Nunes, E. Marega Jr. J. Non-Cryst. Solids **358**,. 399 (2012).
[52] T. Som, B. Karmakar, J. Opt. Soc. Am. B.**26**, B21 (2009).
[53] N.M.Yusoff, Master Thesis (2011), Universiti Teknologi Malaysia, Skudai, Johor.
[54] P. Kellendonk, G. Blasse, Phys Status Solidi (b) **108**, 541 (1981).
[55] D.Rajesh, M.D. Naidu, Y.C.Ratnakaram, J. Phys. Chem. Solids **75**, 1210 (2014).